How hydrological factors initiate instability in a model sandy slope

Tomomi TERAJIMA[a], Ei-ichiro MIYAHIRA[b], Hiroyuki MIYAJIMA[c], Hirotaka OCHIAI[d], and Katsumi HATTORI[e]

a) Disaster Prevention Research Institute, Kyoto University, Gokasho, Uji, 611-0011, Japan.

b) Nippon Engineering Consultant, Co., Ltd., Komagome 3-23-1, Toshima-Ku, Tokyo, 170-0003, Japan.

c) Yokohama Rubber Company, Ltd., Oiwake 2-1, Hiratsuka, 254-8601, Japan

d) Forestry and Forest Products Research Institute, 1 Matsunosato, Tsukuba, 305-8687, Japan.

e) Graduate School of Science, Chiba University, Yayoi-cho 1-33, Inage-ku, Chiba, 263-8522, Japan.

*Corresponding author: Tomomi TERAJIMA, terajima@scs.dpri.kyoto-u.ac.jp

Abstract

Knowledge of the mechanisms of rain-induced shallow landslides can improve prediction of their occurrence and mitigate subsequent sediment disasters. Here, we examine an artificial slope's subsurface hydrology and propose a new slope stability analysis that includes seepage force and the down-slope transfer of excess shear forces. We measured pore water pressure and volumetric water content immediately prior to a shallow landslide on an artificial sandy slope of 32°: the direction of the subsurface flow shifted from downward to parallel to the slope in the deepest part of the landslide mass and this shift coincided with the start of soil displacement. A slope stability analysis that was restricted to individual segments of the landslide mass could not explain the initiation of the landslide; however, inclusion of the transfer of excess shear forces from up-slope to down-slope segments improved drastically the predictability. The improved stability analysis revealed that an unstable zone expanded down-slope with increase in soil water content, showing that the down-slope soil initially supported the unstable up-slope soil; destabilization of this down-slope soil was the eventual trigger of total slope collapse. Initially, the effect of apparent soil cohesion was the most important factor promoting slope stability, but seepage force became the most important factor promoting slope instability closer to the landslide occurrence. These findings indicate that seepage forces, controlled by changes in direction and magnitude of saturated and unsaturated subsurface flows, may be the main cause of shallow landslides in sandy slopes.

Keywords: *shallow landslide, seepage force, flow direction, subsurface hydrology, excess shear force*

INTRODUCTION

Rainfall is recognized as one of the main triggers of shallow landslides (Campbell, 1966; Starkel, 1976; Iverson, 2000), which means that subsurface water is an important consideration when attempting to understand the processes underlying the initiation of shallow landslides. Soil engineering approaches, such as slope stability analyses based on changes in soil stresses and pore water pressure, are the main methods of studying the mechanisms of shallow landslide initiation (Rogers and Selby, 1980; Yagi *et al.*, 1988; Sugano *et al.*, 1989; Rulon *et al.*, 1985; Harp *et al.*, 1990). Theoretical analyses and observations of the movement of soil particles within slopes that have an emerging subsurface flow have been presented (Zaslavsky and Kassiff, 1965; O'Loughlin and Pearce, 1976; Wu *et al.*, 1979; Kochel *et al.*, 1985; Iverson and Major, 1986; Kohno *et al.*, 1987; Selby, 1993; Terajima and Sakura, 1993; Terajima *et al.*, 1997; Terajima *et al.*, 2001; Gabet and Dunne, 2002), and the importance of seepage flow convergence in hillslope hollows with respect to shallow landslide initiation has also been discussed in many studies (Anderson and Burt, 1978; Pierson, 1980; Tsukamoto *et al.*, 1982; Sidle, 1984; Montgomery and Dietrich, 1994; Furuya *et al.*, 1997; Tsuboyama *et al.*, 2000). Iverson and Major (1986) and Reid and Iverson (1992) have shown that ascending subsurface flows at the feet of slopes or at geological boundaries are involved in the initiation of shallow landslides and subsequent debris flows.

The direction of the subsurface flow during rainstorms, which affects driving force for the initiation of shallow landslides, varies temporally and spatially between slopes, so the effects of subsurface flow behavior on the initiation of shallow landslides are yet to be fully clarified for naturally occurring slopes (Iverson, 2000). The effects of subsurface hydrology on not only the movement of soil-particles but also on the initiation of shallow landslides needs to be further examined. Better scientific data on the interaction between the soil and the subsurface hydrology near to and at the time of a shallow landslide will be useful for accurately predicting when shallow landslides are likely to occur and for mitigating subsequent sediment disasters.

There are many factors that cause rainfall-induced landslides, such as increased soil weight due to infiltrated rainwater, increased pore water pressure, decreased apparent soil cohesion, and the appearance of seepage forces resulting from changes in the direction and magnitude of the subsurface flow. Shallow landslide processes are a combination of these factors, which makes it difficult to assess individually the effect of each factor on slope instability. Therefore, to understand quantitatively the process of shallow landslide initiation and the role of each factor in slope instability, we conducted a flume experiment and analyzed the relationship between the subsurface hydrology (pore water pressure, apparent soil cohesion, and seepage force resulting from changes in the soil water content) and the initiation of a shallow landslide. Furthermore, we propose an analytical method for assessing slope instability that takes into account the effect of seepage forces in both saturated and unsaturated conditions and the transfer of excess shear forces down-slope.

EXPERIMENTAL DESIGN

To understand the shallow landslide initiation from the viewpoint of changes in the subsurface hydrology, we examined how to

- calculate the seepage force provided by an unsaturated subsurface flow and to input the seepage force into a slope stability analysis that combines the saturated and unsaturated conditions (refer to Section on Slope Stability Analysis); and

- assess the local shear forces and include the transfer of excess shear forces in the slope stability analysis (refer to Section on Changes in the Factor of Safety in Each Segment of the Shallow Landslide).

Furthermore, to understand quantitatively the detailed landslide process based on our examination of the points above, we also conducted a flume experiment as described below.

Experimental slope

The constructed soil profile and the location of the measurement devices used in the flume experiment are shown in Figures 1 and 2. The steel flume was 9 m long, 4 m high, and 1 m wide, which are scaled dimensions similar to those of naturally occurring slopes. One sidewall of the flume was constructed from reinforced glass to permit observation of soil displacement. The upper, horizontal part of the flume (sections P1 and P2) simulated a ridge. The upper, steep slope (P2–P6) was given a gradient of 32°, which was similar to the angle of internal friction of the sand used in the experiment (Table 1) to ensure that the sand was stable under relatively dry conditions but would allow for landslides after rainfall. The lower, gentle slope (P6–P10) was given a gradient of 10°, which is similar to the angle of internal friction of fluidized sand (Okura et al., 2002). At the lower end of the flume, a stainless steel mesh was placed to allow water to drain from the slope.

The flume was homogeneously filled with sand to a thickness of 0.7 m, and samples were collected from depths of 10 and 30 cm from the ridge, and from depths of 10, 30, and 50 cm from near the lower end of the flume. These two areas were chosen to avoid affecting the initiation of a shallow landslide on the slope between P2 and P6 and buried back after the soil sampling. The physical properties of the five samples were measured and the average values (arithmetic mean) are shown in Table 1.

The density of the sand (ρ_s) was 2.57 g cm^{-3}, the dry density (ρ_d) 1.29 g cm^{-3}, the void ratio (e) 0.99, and the saturated soil water content (measured under statically submerged conditions: θ_{sat}) 0.498. The saturated hydraulic conductivity (K_{sat}), measured by using the variable-head method, was 3.1×10^{-2} cm s^{-1}. The median particle diameter (D_{50}), which was measured with a laser diffraction particle size analyzer (Mastersizer 2000, Malvern Instruments, Ltd., UK), was 0.39 mm. Soil strength was measured by means of the shear box test under both saturated and drained conditions (i.e., the consolidated drained test), and a smaller angle of internal friction (ϕ_{cd}) and soil cohesion (c_{sat}) were shown for the sand compared to the sand under unsaturated conditions, and they were 32.6° and 0 gf cm^{-2}, respectively.

Experimental procedure and the measurement of soil displacement

We filled the flume with the experimental sand on June 13, 2011, and the following day applied a pre-rainfall of 80 mm h^{-1} for 30 min uniformly to the entire slope. On June 15, we conducted the experiment by applying a rainfall of 80 mm h^{-1} until a shallow landslide was observed. Rainfall was simulated by the use of five sprinkler nozzles placed above P1, P4, P6, P8, and P10, of which all are 6.4 m above the lowest part of the flume (the area with the tipping bucket in Fig. 1). We had already confirmed that the sprinkling rate in time and space was homogeneous in our experiment.

We synchronized the measurement of soil displacement and pore water pressure by using time code generators running at 100 Hz. Cylindrical markers were embedded every 20 cm along the length of the flume on the side nearest the reinforced-glass wall at depths of 5, 20, 40, and 60 cm (Fig. 1). The unit weight of the cylindrical markers was 1.60 g cm^{-3}, which corresponds with the wet density of the soil (range: 1.29–1.93 g cm^{-3}), so that the movement of the markers would be linked with that of the soil.

We divided the slope into five sections (P1–P2, P2–P4, P4–P6, P6–P8, and P8–P10) and measured soil displacement by filming the markers from stable points with five digital video cameras (HDR-FX1000, SONY, Japan), each with a resolution of 1440×1080 pixels and 30 frames s^{-1}. We scanned visually the movement of the markers from the video imagery to identify the locus of soil displacement and examined the loci of the markers at various time points prior to shallow landslide.

Pore water pressure, volumetric water content, and the calculation of soil water volume

We measured negative and positive pore water pressures (pressure head) at 100 Hz by using pressure transducers (diameter, 18 mm; range, 70 kPa; accuracy, 0.015%; Model PDCR800, Druck Co., Ltd., UK) with glass filters attached to the tips. The pore water pressure gauges were positioned vertically and parallel to the slope at depths of 10, 40, and 65 cm at each sampling point (Figs. 1 and 2a).

As shown in Figure 2a, we divided the upper-slope's profile (P1–P7) into triangles based on the position of the pore water pressure gauges to calculate the hydraulic gradient (i.e., the direction of the subsurface flow and seepage force) and the soil water content in the triangles (i.e., soil weight and apparent soil cohesion). Because the width of the slope must also be taken into account, these segments were actually considered to be triangular columns amenable to three-dimensional analysis.

The pore water pressure in each triangle segment in Figure 2a was calculated as the average of the pore water pressure at the three corners of the triangle. The volumetric water content (VWC) of the square columns located in the shallow soil less than 10 cm deep was considered to be under the control of the triangular columns immediately below them. Based on direct measurement at 1-min intervals of both the VWC with probe sensors (ECHO-5TE, Decagon Device, USA) and the pore water pressures in P1, a graph of the relationship between VWC and pore water pressure (a soil water retention curve for the experimental soil under infiltration; i.e., irrigation process), as shown in Figure 3, was used to determine the VWC of all of the triangle segments. Figure 3 shows that, in the discussion (chapter 4), we do not have to consider the phenomenon of hysteresis in the relationship between soil water content and pore water pressure.

When we calculated VWC at a time series shown in Figures 9 and 10 (at the onset of rainfall and at 60, 50, 40, 30, 20, 10 min and 1 sec prior to landslide), the pressure head corresponding to the range of white circles in Figure 3 (between -1.07 and 4.00 cmH_2O) was hardly recorded. Thus, on account of simplification to calculate VWC in the stability analysis, we applied a curve fitting to the relationship between the pressure head below -1.07 cmH_2O and VWC below 0.316 (black circles, white triangles, and crosses in Figure 3) and obtained a correction curve expressed as $y = 0.11 + 0.24\, e^{0.23x}$ under the correlation coefficient of 0.99. Instead of the models based on Brooks and

Corey (1964) or van Genuchten (1980), this correction curve was applied in our analysis to calculate VWC under unsaturation below -1.07 cmH_2O. As shown in Figure 3, the VWC corresponding to 0 cmH_2O under infiltration (i.e., irrigation process) was about 0.330. However, during infiltration in the experiment, the saturated VWC at the pressure head more than 4 cmH_2O was mostly same as θ_{sat}. This fact indicates that, when considering the movable soil water concerning seepage force of unsaturated flow (Equation 10 in the Section on Slope Stability Analysis), we should apply θ_{sat} measured under the statically submerged condition.

The weight of the water and soil in the landslide mass was obtained by summation of each value in each triangle segment. When the landslide mass only included part of a triangle segment (Fig. 2a), we calculated the ratio of the area of the landslide mass to the total segment area, and multiplied this ratio by the soil water content in the triangle segment to calculate the soil water volume in the relevant part of the landslide mass.

We assumed that shallow landslides have a uniform horizontal geometry above the sliding surface because, prior to landslide occurrence, mostly horizontal, linear tension cracks were formed at the top of the landslide mass. Furthermore, the change in soil volume caused by the soil displacement, which was calculated individually for each triangle segment, was a few percent of the original volume (less than ±10 % and the landslide mass was compressed overall only -3.1% on average at 1 sec prior to landslide; refer to Fig. 5 and the Section on Soil Displacement and Subsurface Flow). Thus, we assumed that the volume of the landslide body did not change during the experiment and that the effects of soil displacement on changes in pore water pressure and on VWC in the landslide mass were very small. Although soil generally shows an elastic–plastic behavior, the landslide mass in our study mostly kept its original form until landslide occurrence. Therefore, when we discuss the experimental results on the basis of particle dynamics, the changes in normal and shear stresses in the landslide mass are calculated to understand the importance of seepage flow under the hypothesis that the landslide mass is a rigid body.

RESULTS

Landslide features and pore water pressure

A shallow landslide occurred 1 h, 41 min, 33 s (6093 s) after the onset of rainfall, by which time a total rainfall of 135.4 mm had been applied to the flume. The entire slope between P3 and P6 completely collapsed to the maximum depth of 0.7 m (Fig. 2). The loading of the landslide mass on the lower-slope caused the fluidization at the lower-slope, which accounts for the excess pore-water pressure (Fig. 4) by the higher soil water content (wide saturated area) of the lower-slope (see Fig. 6b for the groundwater table which was defined by the pressure head of 0 cmH_2O). About 60% of the landslide mass and 80% of the sliding surface were saturated at 1 s prior to landslide occurrence (Fig. 6b).

The average pore water pressure in each section (Fig. 4) was greater than −50 cmH_2O at the onset of rainfall, indicating that the VWC of the slope was within field capacity throughout the experiment. This means that from the start of the experiment, subsurface flow was affected by gravity. Pore water pressure at most points of the slope increased almost immediately at the onset of rainfall to about −10 cmH_2O and remained stable after the passing of the wetting front; this was especially prominent in the shallower soil. The wetting front reached a depth of 65 cm within 60 min of the onset of rainfall (more than 40 min prior to landslide). Pore water pressure at depths of 10 and 40 cm briefly remained stable after the passing of the wetting front and then rose distinctly at depths of 40 and 65 cm in sections P3－P9, whereas at a depth of 10 cm, it remained stable. Excess pore water pressure was generated at a depth of 65 cm in sections P4 and P5 after the shallow landslide occurrence, which can be attributed to the sudden compaction of the soil caused by the loading of the upper landslide mass. This was also true in the lower-slope (P6 to P10) at depths of 40 and 65 cm.

Soil displacement and subsurface flow

Soil displacement (loci of the markers) and the rate of areal change in triangles in the upper, steep slope, based on the position of the cylindrical markers, are shown in Figure 5. Soil displacement was not observed until 50 min prior to landslide occurrence (50 min after the onset of rainfall; Fig. 5a). Soil displacement was distinctly recognized between 50 and 40 min prior to landslide (between 50 and 60 min after the onset of rainfall), and the areal changes in the triangles were appeared at that time (Fig. 5b). Thus the volumetric change in soil of the upper, steep slope was less than ±10% up to landslide occurrence and that in the landslide mass at 1 sec prior to landslide was estimated at overall only -3.1% (compression) on average. The data on the pressure heads (Fig. 4) did not clearly show that soil displacement had any effect on pore water pressure. These findings suggest that the very slow change in soil volume by only a few percent did not produce the substantial changes observed in pore-water pressure.

Temporal changes in the equi-potential lines and the direction of the subsurface flow prior to the landslide are shown in Figure 6. The flume was homogeneously filled with sand (Section on Experimental Slope). Thus, even though we conducted the experiment under a relatively coarse system of pressure gauges, the linear interpolation (proportional allotment) between pressure gauges, used software (Surfer; Golden Software Inc., USA), allowed us to provide the smooth pattern of equi-potential lines. At 40 min prior to landslide (about 60 min from the onset of rainfall; Fig. 6a), the saturated area grew larger in the deep soil of the lower, gentle slope (P6–P10) and the upper sections of the upper, steep slope (P3–P4) after the wetting front passed, and tension cracks developed between P1 and P2. In contrast, in the shallower soil of the upper, steep slope (P3–P6), the soil displacement almost parallel to the slope was occurred between 50 and 40 min prior to landslide (Fig. 5a).

The direction of the subsurface flow began to change between 50 to 40 min prior to landslide (at 50 to 60 min after the onset of rainfall), obviously in the deep soil and slightly in the shallow soil in sections P3 and P4 (Fig. 6a), and the timing of the first directional change in subsurface flow coincided mostly with the beginning of soil displacement. Between 40 min and 1 s prior to the landslide, except at the ridge (P1 and P2), the subsurface flow direction in most sections changed from downward as in Figure 6a to nearly parallel to the slope as in Figure 6b, not only below the groundwater table but also above it in the unsaturated area close to the groundwater table in the shallow part of the soil.

DISCUSSION

Analytical theory

The beginning of soil displacement coincided nearly with the timing of the first directional change in subsurface flow. Therefore, factors that are related to changes in the direction and magnitude of the subsurface flow (e.g., seepage force) could be related to both the soil displacement and the subsequent shallow landslide observed during the experiment. This suggests that it may be necessary to take seepage force into account when attempting to elucidate the mechanism of landslide initiation, create models of landslide processes, or develop measures to predict the timing of shallow landslide occurrence. We present below an analytical method that takes into account the effect of seepage force, as well as the transfer of excess shear force, on landslide initiation.

Modified Fellenius method

Measurement of normal and shear forces in landslide masses allows evaluation of landslide dynamics. Figure 7 shows two-dimensional schematic illustrations of the forces affecting the sliding surface of a shallow landslide mass. The modified Fellenius method (Fellenius, 1927; Fig. 7a) has long been used for the analysis of the slope stability that has free groundwater tables. Utilizing the modified Fellenius method, the landslide mass is divided into slices and the shear force in a slice affecting the sliding surface (S) is given by

$$S = W_t \sin \alpha, \quad (1)$$

where W_t is the total weight of the slice (soil + subsurface water) and α is the average slope of the sliding surface. Similarly, the normal force affecting the sliding surface (N) is given by

$$N = W_g \cos \alpha, \quad (2)$$

where W_g is the effective weight of the shallow landslide mass, including infiltrated rain water, which is expressed by

$$W_g = W_t - u = (\rho_d g V_{unsat} + \rho_w g V_{unsat} \theta_a + \gamma_{sat} V_{sat}) - \rho_w g V_{sat}$$

$$= (\rho_d g + \rho_w g \theta_a) V_{unsat} + (\gamma_{sat} - \gamma_w) V_{sat}, \quad (3)$$

where u is buoyancy; ρ_d is the dry density of the soil; g is the gravitational acceleration; V_{unsat} is the soil volume of the unsaturated area in the slice; ρ_w is the water density; θ_a is the actual VWC at any time, which is defined by pore water pressure (refer to Fig. 3); γ_{sat} is the unit volumetric weight of the saturated soil; V_{sat} is the soil volume of the saturated area; and γ_w is the unit volumetric weight of the water. The first term on the right-hand side of Equation 3 [i.e., $(\rho_d g + \rho_w g \theta_a)V_{unsat}$] represents the combined weight of the soil and water in the unsaturated part of the slice, whereas the second term [i.e., $(\gamma_{sat} - \gamma_w)V_{sat}$] represents the effective weight of the soil in the saturated part of the slice, which is affected by buoyancy. In Equation 3, $\gamma_{sat} - \gamma_w$ can alternatively be expressed as

$$\gamma_{sat} - \gamma_w = (\rho_s - \rho_w) / (1 + e), \quad (4)$$

where ρ_s is the soil density and e is the void ratio.

For the analysis of slope stability, Equations 1 and 2 provide the factor of safety based on the modified Fellenius method (FS_{mF}) such that

$$FS_{mF} = (c\, A \cos^{-1}\alpha + N \tan\phi) / S, \quad (5)$$

where c is the soil cohesion, which is variable depending on VWC as shown by Equation 6, A is the plan area of the slice, and ϕ is the angle of internal friction of the soil. The angle of internal friction is usually invariable in sandy materials when the degree of saturation is greater than 20% (Matsushi and Matsukura, 2006). This indicates that it is unnecessary to take into account the change in ϕ in our experiment, because the VWC calculated from Figures 3 and 4 was always greater than 0.10 under the saturated VWC (θ_{sat}) of 0.498, meaning that the degree of saturation of the soil was always greater than 20%.

The cohesion of the soil was 0 gf cm^{-2} when saturated (Table 1). Therefore, under unsaturated conditions, the apparent soil cohesion is mainly affected by VWC (i.e., suction) and can be expressed as

$$c = \rho_w g \ \varphi, \tag{6}$$

where φ is the suction calculated at the intersections between the sliding surface and the sides of the triangles, at which the pressure head was proportionally assigned by using the pressure heads obtained at the two measurement points (vertexes) of the corresponding sides of the triangles.

Slope stability analysis taking into account the seepage force, apparent soil cohesion, and slope of sliding surface

In our experiment, the packed sand did not collapse into the vertical boreholes (depth, 70 cm; diameter, 10 cm) that were made to install the observation sensors. This indicates that the soil water conditions before the rainfall supply did not promote the interaction of stresses between sections, and therefore, that at the beginning of the experiment, it is likely that the down-slope sections were not affected by up-slope stresses.

To take into account the difference in pore water pressure between the up-slope and down-slope edges of a slice of landslide mass, Equation 1 can be modified and the effective shear force calculated as

$$S = W_t \sin \alpha + \Delta H \cdot \cos \alpha, \tag{7}$$

where ΔH is the difference in pore water pressure between the up-slope (H_1) and down-slope (H_2) edges of a slice (see Fig. 7a). However, when $\Delta H \leq 0$ (i.e., $H_1 \leq H_2 < H_1 + A \tan \alpha$), the effect of pore water pressure on shear force can be disregarded because it causes the reverse effect (i.e., a decrease in S), even though there is still subsurface flow and seepage forces still exist in the landslide mass. This implies that Equation 7, based on the modified Fellenius method, cannot be applied universally in slope stability analyses.

Howard and Mclane (1988) conducted experiments on spring sapping by using simulated slopes and showed that the hydraulic gradient and the direction of the saturated subsurface flow was related to the movement of soil particles. In our experiment, soil displacement began after the wetting front arrived at the deepest soil, which coincided mostly with a directional change in subsurface flow (Fig. 6a). This indicates that directional changes in subsurface flow may be the main cause of soil displacement, and subsequently a shallow landslide. We therefore must consider the changes in normal and shear stresses by including seepage force in the evaluation of the effective force affecting landslide mass. Thus, instead of using only the difference in pore water pressure (i.e., $\Delta H \cdot \cos \alpha$) in Equation 7, a function that also takes into account seepage force should be applied to the stability analyses of shallow landslides involving a free groundwater table.

Cedergren (1977) showed that seepage force affecting saturated soil was proportional to the hydraulic gradient of the subsurface flow, which can be expressed as

$$SF_{\mathrm{sat}} = \rho_{\mathrm{w}}\, g\, i_{\mathrm{sat}}, \tag{8}$$

where SF_{sat} is the seepage force for an unit volume of soil with saturated subsurface flow and i_{sat} is the hydraulic gradient under saturated conditions. The position of the pore water pressure gauges in our experiments (vertical and parallel to the slope; Figs. 1 and 2a) allowed the use of the measured pore water pressures to calculate the hydraulic gradient and facilitate the calculation of changes in the normal and shear forces due to the seepage force resulting from changes in direction and magnitude of subsurface flow.

As shown in Figure 7b, the equation for normal force taking seepage force into account is derived from the fraction of the vertical force in the normal direction. The seepage force in a vertical (gravitational) direction affecting the sliding surface (SF_g) is calculated according to the following equations:

$$SF_g = \rho_w g \{ n^{-1} \sum (i_g \beta)\} V_L / (1 + e), \quad (9)$$

where n is the number of triangle sections included in the slice (see Fig. 2a), i_g is the hydraulic gradient in the vertical (gravitational) direction in each triangle section, β is the coefficient used to calculate the seepage force from the hydraulic gradient depending on the water condition (i.e., saturated or unsaturated) and is defined by Equation 10 below, and V_L is the total volume of the landslide mass in the slice. In Equation 9, $n^{-1} \sum (i_g \beta)$ and $V_L / (1 + e)$ represent the average vertical hydraulic gradient and the effective volume of the slice that is affected by the seepage force, respectively.

Soil water at water contents exceeding the suction of 50 cmH_2O is immovable by gravity and consequently does not contribute to the seepage force because it is mostly retained and adsorbed in soil pores. Thus, we can use the coefficient β to account for the reduction in the seepage force by the unsaturated subsurface flow at water contents between the suction of 0 and 50 cmH_2O, which is given by

$$\beta = (\theta_a - \theta_{swc=50}) / (\theta_{sat} - \theta_{swc=50}), \quad (10)$$

where $\theta_{swc=50}$ is the VWC at a suction of 50 cmH_2O and θ_{sat} is the saturated VWC (0.498) obtained under both infiltration in the landslide experiment and statically submerged conditions in the laboratory experiment (Fig 3). The coefficient β is variable according to the change in VWC within the field capacity represented by the VWC at a suction between 0 and 50 cmH_2O; i.e., from $\beta = 1$ for saturated soil ($\theta_a = \theta_{sat}$) to $\beta = 0$ for unsaturated soil with a VWC at a suction exceeding 50 cmH_2O ($\theta_a \leq \theta_{swc=50}$).

Dividing the SF_g obtained by using Equation 9 by the normal direction gives

$$SF_n = SF_g \cos \alpha, \tag{11}$$

where SF_n is the seepage force fraction of the vertical seepage force in the normal direction. The effective normal force (N_e) applied to the seepage force is given by

$$N_e = N + SF_n \ (= W_e \cos \alpha), \tag{12}$$

where W_e is the effective weight of the landslide mass applied to the effect of the vertical seepage force.

As shown in Figure 7b, when we consider the vertical seepage force (SF_g), the effective weight of the soil is expressed not by W_t as with the modified Fellenius method (Fig. 7a), but by

$$W_e = W_t - u + SF_g = W_g + SF_g. \tag{13}$$

Thus, the effective shear force (S_e') affected by W_e is expressed by

$$S_e' = W_e \sin \alpha. \tag{14}$$

Eventually, the effective shear force parallel to the sliding surface (S_e) is expressed not by S as shown in Figure 7a, but by

$$S_e = S_e' + SF_s = W_e \sin \alpha + SF_s, \tag{15}$$

where SF_s is the seepage force parallel to the sliding surface, which is given by

$$SF_s = \rho_w\, g\ \{\ n^{-1} \sum (i_s\beta)\} V_L\ /\ (1 + e), \tag{16}$$

where i_s is the hydraulic gradient parallel to the sliding surface. In Equation 16, $n^{-1} \sum (i_s\beta)$ represents the average hydraulic gradient parallel to the sliding surface and $V_L / (1 + e)$ represents the effective volume of a slice that is affected by the seepage force parallel to the sliding surface.

Finally, Equations 6, 12, and 15 provide a factor of safety that takes into account the effect of seepage force on internal forces in the directions both normal and parallel to the sliding surface, as

$$FS_e' = (c\, A \cos^{-1} \alpha + N_e \tan \phi)\ /\ S_e, \tag{17}$$

where FS_e' is the factor of safety that takes into account apparent soil cohesion and seepage force, but not the transfer of excess shear force described by Equation 18. When the FS_e' of a slice is below 1.0, the excess shear force that should be transferred to the adjacent down-slope landslide segment (S_{exc}) can be expressed as

$$S_{exc} = S_e - (c\, A \cos^{-1} \alpha + N_e \tan \phi), \tag{18}$$

According to the interrelationship regarding the slope of sliding surfaces (α) between the slices as shown in Figure 8, S_{exc} is categorized as follows:

Case 1 : under $\alpha_1 = \alpha_2$; $S_x = S_{exc} \cos \alpha_1 = S_{exc} \cos \alpha_2$ (19-1)

Case 2 : under $\alpha_1 > \alpha_2$; $S_x = S_{exc} \cos (\alpha_1 - \alpha_2)$ (19-2)

Case 3 : under $\alpha_1 < \alpha_2$; $S_x = S_{exc} \cos (\alpha_2 - \alpha_1)$ (19-3)

Case 4 : under the reverse slope in α_2 ; $S_x = S_{exc} \cos (\alpha_1 + \alpha_2)$ (19-4)

where S_x is the excess shear force that is transferred from the adjacent up-slope landslide segment. Thus, the factor of safety of the landslide segment included in the slice can be calculated in order as

$$FS_e = (c\,A\cos^{-1}\alpha + N_e \tan\phi) / (S_e + S_x), \quad (20)$$

where FS_e is the factor of safety that takes into account the effect of apparent soil cohesions, pore water pressures (buoyancy), seepage forces, and the transfer of excess shear forces from the adjacent up-slope landslide segment.

Changes in the factor of safety in each segment of the shallow landslide

The changes in the factor of safety calculated from Equations 17 and 20 are shown in Figure 9. Segment 1, the upper-most section of the landslide mass between P2 and P3, did not receive any excess shear force from the section of the slope between Segment 1 and P2. The factor of safety without accounting for excess shear force (FS_e') in Segment 1 at 1 s prior the shallow landslide was 0.996, showing that the timing of the shallow landslide corresponded to the FS_e' falling below 1.0. This shows that the slope stability analysis we propose in the Section on Slope Stability Analysis can be adapted to examine the landslide process at the upper-most parts of landslide masses.

In Segment 2, which is the upper part of the landslide mass between P3 and P4, because the small excess shear force from Segment 1 was only transferred 1 s prior to the shallow landslide, the change in FS_e' mostly coincided with the factor of safety that accounts for excess shear force (FS_e). The FS_e' stayed below 1.0 from the onset of rainfall, showing that slope instability was already present at the onset of rainfall. This is likely due to the pre-rainfall applied the previous day (80 mm h^{-1} for 30 min), and a landslide in Segment 2 at the early stages of the experiment was likely prevented only by the strength of the down-slope soil (Segments 3–5). Similarly in Segment 3, which is in the middle of the slope between P4 and P5, the FS_e' fell below 1.0 between 50 and 60 min after the onset of rainfall (between 50 to 40 min prior to the shallow landslide); however, when taking into account the transfer of excess shear force from Segment 2, slope instability (FS_e < 1.0) occurred earlier between 0 and 40 min after the onset of rainfall (about 80 min prior to the shallow landslide). Again, this shows that Segment 3 was likely supported by the strength of the down-slope soil (Segments 4 and 5), which delayed soil collapse.

In contrast, the factors of safety of Segments 4 and 5, the most down-slope landslide mass between P5 and P7, were greater than 1.0 until immediately before the shallow landslide occurred. In Segment 4, while FS_e' and FS_e were 2.133 and 1.013 at 10 min prior to the shallow landslide, they fell to 1.789 and 0.898 at 1 s prior to the shallow landslide, respectively. Similarly, in Segment 5, FS_e' and FS_e at 1 s prior to the shallow landslide were 3.456 and 1.014. This further shows that the transfer of up-slope excess shear force corresponded with the occurrence of the shallow landslide and with the FS_e falling below 1.0.

The stability analysis we propose here explains the process of shallow landslide initiation in the current experiment as follows:

1) Slope instability partially occurred up-slope in the early stages of the experiment (within 40 min after the onset of rainfall); however, a shallow landslide was prevented due to the down-slope soil being strong enough to stabilize the total landslide body.

2) The instability of the total landslide body and subsequent shallow landslide were eventually promoted when the down-slope FS_e of the landslide mass fell below 1.0, which was at around 100 min after the onset of rainfall (a few seconds prior to the shallow landslide).

Our slope stability analysis based on Equation 20 takes into account the effect of apparent soil cohesion, changes in the effective weight of the soil, seepage forces under unsaturated and saturated soil water conditions, and the down-slope transfer of excess shear forces. The current results show that this slope stability analysis is adaptable to and useful for examining the shallow landslide process in sandy materials.

Assessment of the hydrological factors that promote landslide initiation

To understand the effects of hydrological factors (i.e., apparent soil cohesion, seepage force, and pore water pressure) on landslide initiation, we considered the changes in FS_e' over time and the factor of safety in which one of the three factors was eliminated from Equation 17. The transfer of excess shear force from an up-slope to a down-slope segment greatly affected the change in shear force in the down-slope segment and provided a relatively small difference between FS_e and the factor of safety in which one of the factors had been eliminated. Additionally, it is difficult to compare in a straightforward manner the segments that did not receive up-slope excess shear forces (Segments 1 and 2) with those segments that did (Segments 3, 4, and 5). Therefore, FS_e' was used in Figure 10 as the criterion to assess the change in the factor of safety as a result of eliminating one of the hydrological forces.

In Segment 1, which remained unsaturated throughout the experiment, FS_e' was markedly reduced by not taking into account apparent soil cohesion. Similarly, in Segments 2 to 4 during the early stages of the experiment, the unsaturated conditions in the segments meant that not taking into account apparent soil cohesion markedly reduced the FS_e'; however, in the later stages of the experiment (near the occurrence of the shallow landslide), not taking into account seepage force produced the biggest difference in the value of FS_e'. In Segment 5, we were unable to calculate seepage force because there was only one pressure gauge in the segment; however, due to the biggest difference from FS_e', it is possible that the change in pore water pressure was more important factor affecting shallow landslide occurrence than that in the apparent soil cohesion.

These results indicate that, because taking the seepage force into account reduced the factor of safety of the slope, seepage forces strongly influence the initiation of shallow landslides and possibly affect the beginning of soil displacement, which corresponds with a change in direction of the subsurface flow. An experiment conducted on the slope of a granitic mountain (Ochiai *et al.*, 2004) where simulated rainfall (80 mm h^{-1} for 7 h) induced a shallow landslide, revealed that a change in direction of the subsurface flow coincided with the beginning of soil displacement, and the change in direction of the subsurface flow was assumed to be the main factor for initiating the shallow landslide. These results, together with those we present here, show that accounting for subsurface flow (seepage force) allows for better prediction of the timing of shallow landslide initiation, indicating that the effect of seepage force on slope instability under both saturated and unsaturated conditions is important in slope stability analyses.

CONCLUSIONS

The following are the major findings obtained from our flume experiment and analysis of shallow landslide initiation:

1) The direction of subsurface flow in landslide bodies begins to change from downward

to parallel to the slope prior to the occurrence of a shallow landslide, and the timing of this change coincides with the beginning of soil displacement.

2) The slope stability analysis that we propose here shows that slope instability occurs partially in the up-slope section of the landslide body during the early stages of development of conditions that facilitate a shallow landslide (within 40 min after the onset of rainfall); however, a shallow landslide does not occur then because the strength of the down-slope soil supports the unstable upslope section.

3) Instability of the total landslide body and the subsequent shallow landslide were promoted when the factor of safety for the down-slope section of the landslide body fell below 1.0, which was at around 100 min after the onset of rainfall (1 s prior to landslide occurrence).

4) Seepage forces markedly affect the promotion of shallow landslide initiation and are therefore important in slope stability analyses.

Few studies of landslides have considered the effect of seepage forces through either saturated subsurface flow or unsaturated subsurface flow. However, by considering seepage force, the prediction accuracy for the timing of landslide occurrence may be improved compared with predictions based on changes in soil strength resulting from changes in soil weight and soil water content via rainwater infiltration.

ACKNOWLEDGEMENT

The present study was based both on a Master’s thesis in the Graduate School of Science and Technology, Chiba University, written by H. Miyajima in 2008 and on a Master’s thesis in the Graduate School of Science, Kyoto University, written by E. Miyahira in 2012. In addition, the present study was funded by a grant for environmental research from the Sumitomo Foundation, Japan (No. 103098).

Figure 1. Experimental flume and measurement devices

Figure 2. Slope segments (a) to calculate the hydraulic gradient and soil water content in

Figure 3. Relationship between the volumetric water content (VWC) and pressure heads

Figure 4. Changes in pore water pressures.

Figure 5. Soil displacement (loci of the markers) at P2 – P6 at 50, 40, 30, 20, 10, and 1

Figure 6. Temporal changes in the equi-potential lines and the directions of subsurface

Figure 7. Schematic illustrations related to inner forces affecting a slice of landslide

Figure 8. Types of the interrelationship regarding the slope of sliding surface between

Figure 9. Changes in the factor of safety. FS_e' (eq.17) is the factor of safety not taking

Figure 10. Effects of each force on shallow landslide initiation. FS_e' (eq.17) is the factor

Table 1. Physical properties of the experimental sand (arithmetic mean of 5 samples)

REFERENCES

Anderson MG, Burt TP. 1978. The role of topography in controlling through flow generation. *Earth Surface Processes & Landforms* **3** : 1331–344.

Brooks RH, Corey AT. 1964. Hydraulic properties of porous media: *Hydrology. Papers. 3, Civil Engineering Department, Colorado State University, Fort Collins.*

Campbell AP. 1966. Measurement of movement an earth flow. *Soil Water* **2** : 23–24.

Cedergren HR. 1977. Seepage, drainage and flow nets: 2nd ed. John Wiley and Sons : New York; 534.

Fellenius W. 1927. Erdstatische Berechnung : Berlin : W. Ernst und Shon.

Furuya G, Sassa K, Fukuoka H, Hiura H. 1997. The relationship between underground erosion and landslide movement in a crystalline schist landslide, Zentoku, Tokushima, Japan. *Jour. Jpn. Landslide Soc*. **34** : 9–16. (in Japanese with an English abstract and captions)

Gabet EJ. Dunne T. 2002. Landslide on coastal sage-scrub and grassland hillslopes in a severe El Nino winter. The effects of vegetation conversion on sediment delivery. *Geological Soc. America Bull.* **114** : 983–990.

Harp EL, Wells WG, Sarmiento G. 1990. Pore pressure response during failure in soils. *Geol. Soc. Am. Bull.* **102** : 428–438.

Howard AD, Mclane CF. 1988. Erosion of cohesionless sediment by groundwater seepage. *Water Res. Res.* **24** : 1659–1674.

Iverson RM, Major JJ. 1986. Groundwater seepage vectors and the potential for hillslope failure and debris flow mobilization. *Water Res. Res.* **22** : 1543–1548.

Iverson RM. 2000. Landslide triggering by rain infiltration. *Water Res. Res.* **36** : 1897–1910.

Kochel RC, Howard AD, Maclane CF. 1985. Channel networks developed by groundwater sapping in fine-grained sediments. *Analogs to some Martin Valleys.* In Woldenberg, M.J. (ed.), Models in Geomorphology. Allen and Unwin: Boston ; 313–341.

Kohno I, Nishigaki, M, Takeshita, Y. 1987. Levee failure caused by seepage and preventive measures. *Natural Disaster Science* **9** : 55–76.

Matsushi Y, Matsukura Y. 2006. Cohesion of unsaturated residual soils as a function of volumetric water content. *Bull. Eng. Geol. Env.* **65** : 449–455.

Montgomery DR, Dietrich WE. 1994. A physically based model for the topographic control on shallow landsliding. *Water Res. Res.* 30 : 1153–1171.

Ochiai H, Okada Y, Furuya G, Okura Y, Matsui T, Sammori T, Terajima T, Sassa K. 2004. A fluidized landslide on a natural slope by artificial rainfall. *Landslides* **1** : 211–219.

Okura Y, Kitahara H, Ochiai H, Sammori T, Kawanami A. 2002. Landslide fluidization process by flume experiments. *Engineering Geology* **66** : 65–78.

O'Loughlin CL, Pearce AJ. 1976. Influence of Cenozoic geology on mass movement and sediment yield response to forest removal, North Westland, New Zealand. *Bull. Int. Assoc. Eng. Geology* **14** : 41–46.

Pierson TC. 1980. Piezometric response to rainstorms in forested hillslope drainage depressions. *J. Hydrol. N.Z.* **19** : 1–10.

Reid ME, Iverson RM. 1992. Gravity-driven groundwater flow and slope potential 2. Effect of slope morphology, material properties, and hydraulic heterogeneity. *Water Res. Res.* **28** : 939–950.

Rogers NW, Selby MJ. 1980. Mechanisms of shallow translational landsliding during summer rainstorms, North Island, *New Zealand. Geograf. Ann.* ***62A*** : 11-21.

Rulon JJ, Rodway R, Freeze RA. 1985. The development of multiple seepage faces on layered slopes. *Water Res. Res.* **21** : 1625–1636.

Selby MJ. 1993. Hillslope materials and processes, 2nd-ed. Oxford Univ. Press: Oxford; 451p.

Sidle RC. 1984. Shallow groundwater fluctuations in unstable hillslopes of coastal Alaska. *Zeitschlift fur Gletscherkunde und Glazialgeology* **20** : 79–95.

Starkel L. 1976. The role of extreme (catastrophic) meteorological events in the contemporary evolution of slopes. *In Geomorphology and Climate*, edited by E. Derbyshire. John Wiley & Sons: New York; 203–246.

Sugano Y, Matsumoto E, Terashima H. 1989. Rainfall experiment on the behavior of subsurface water in slope soil layers. *Bulletin of The Environmental Research Center, The University of Tsukuba* **13** : 45–53. (in Japanese)

Terajima T, Sakura Y. 1993. Effect of subsurface flow on a topographic change at a valley head of granitic mountains. *Trans. Jpn. Geomorph. Union* **14** : 365–384. (in Japanese with English abstract and captions).

Terajima T, Sakamoto T, Nakai Y, Kitamura K. 1997. Suspended sediment discharge in subsurface flow from the head hollow of a small forested watershed, northern Japan. *Earth Surf. Processes and Landf.* **22** : 987–1000.

Terajima T, Sakamoto T, Shirai T. 2001. Bed load yield caused by subsurface water discharge in a forested 0-order basin in Hokkaido, Northern Japan. *Trans. Jpn. Geomorph. Union* **22** : 1–22. (in Japanese with English abstract and captions)

Tsuboyama Y, Sidle ,RC, Noguchi S, Murakami S, Shimizu T. 2000. A zero-order basin – its contribution to catchment hydrology and internal hydrological processes. *Hydrological processes* **14** : 387–401.

Tsukamoto Y, Ohta T, Noguchi H. 1982. Hydrological and geomorphological studies of debris slides on forested hillslopes in Japan. *IAHS publ.* : **137**: 89–98.

van Genuchten M. 1980. A closed-form equation for predicting the hydraulic conductivity of unsaturated soils: *Soil Sci. Soc. of America Jour.* **44**: 892-898.

Wu TH, McKinnel WP, Swanson DN. 1979. Strength of tree roots and landslides on

Prince of Wales Island, Alaska. *Canadian Geotech. Jour.* **16** : 19–33.
Yagi N, Enoki A, Yatabe R. 1988. Prediction of failure of sandy slopes during rain. *Proc. Symp. Landslide Mechanisms and Measures, Shikoku Branch of Jpn. Geotech. Soc.* : 37–42.(in Japanese)
Zaslavsky D, Kassiff G. 1965. Theoretical formulation of piping mechanism in cohesive soils. *Geotechnique* **15** : 305–316.

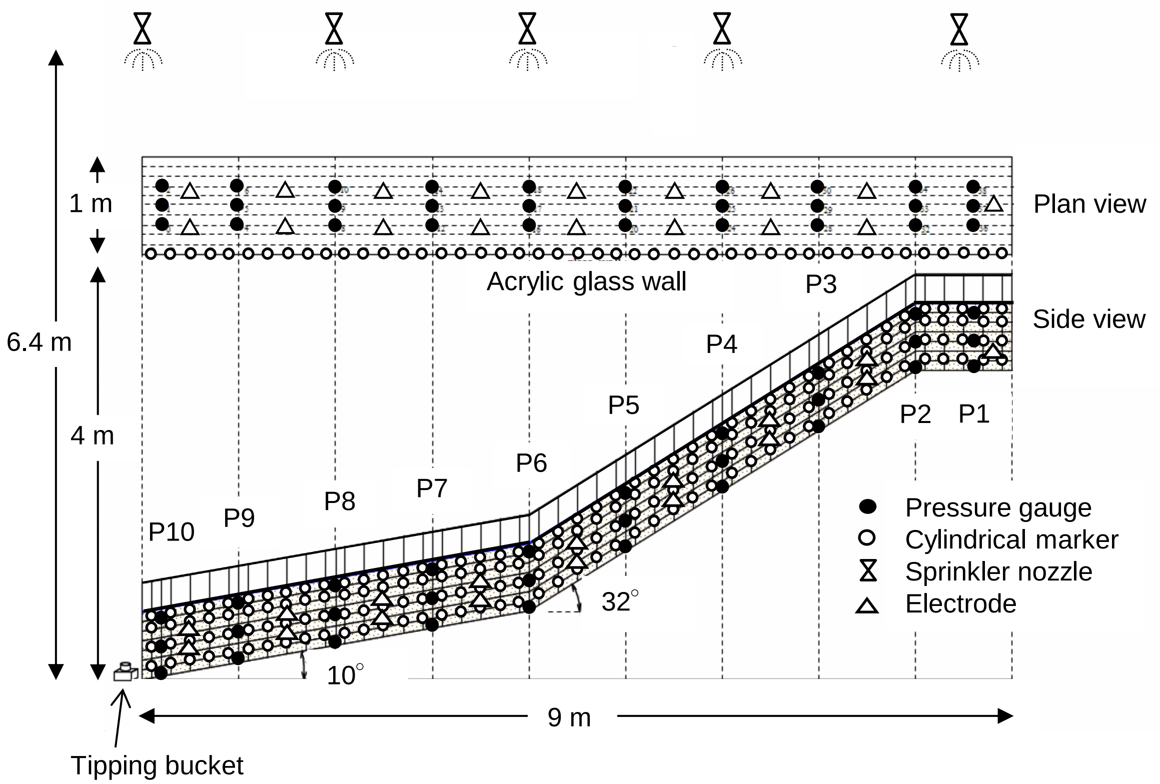

Figure 1. Experimental flume and measurement devices

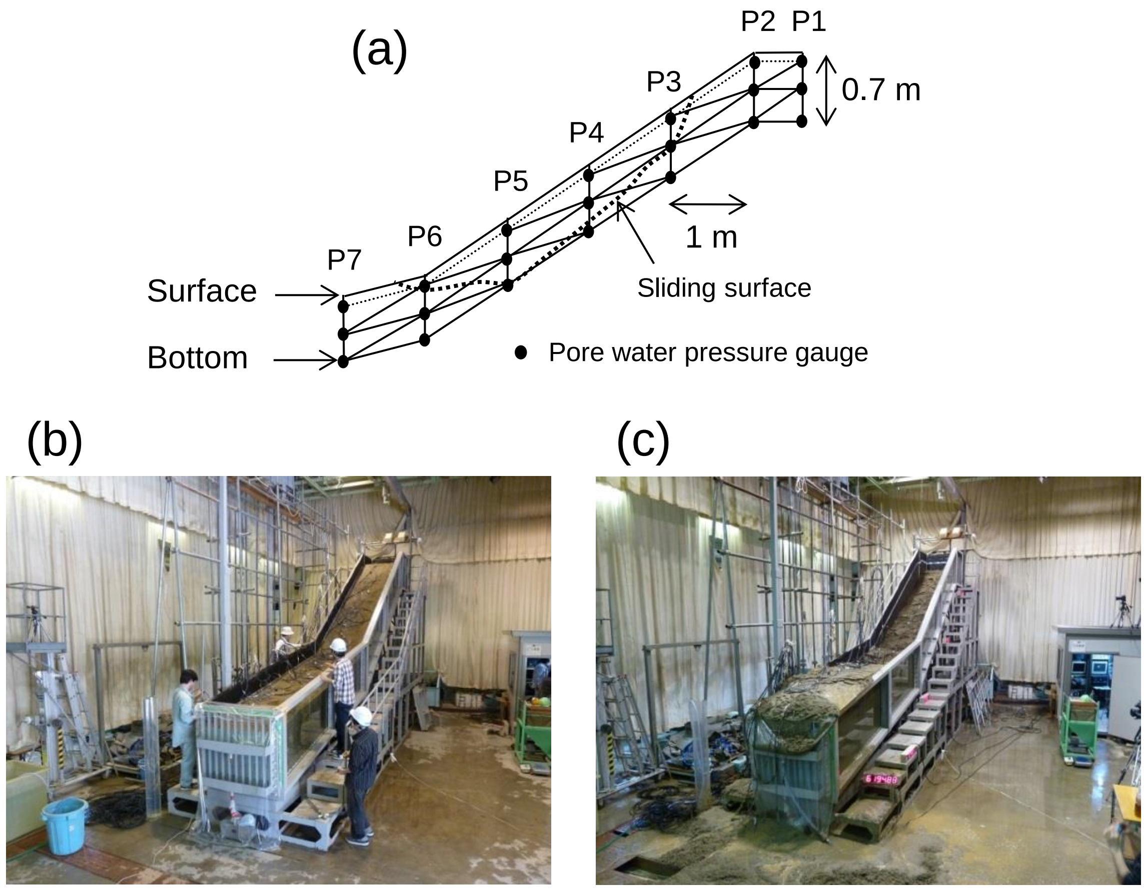

Figure 2. Slope segments (a) to calculate the hydraulic gradient and soil water content in the landslide mass and consequently to examine soil weight and changes in direction of subsurface flows, and photographs of the experiment before (b) and after landslide (c).

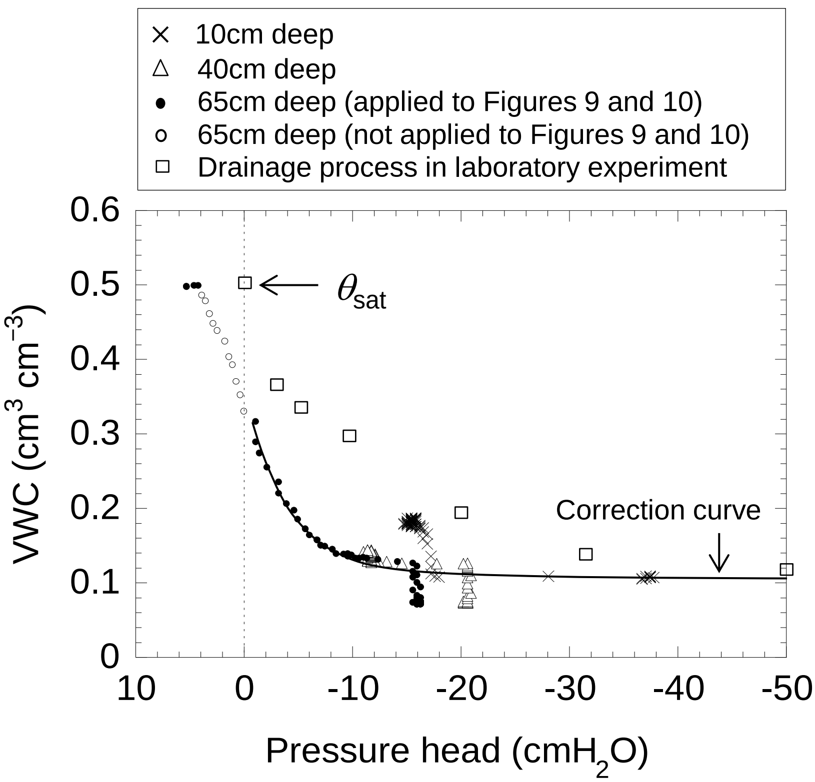

Figure 3. Relationship between the volumetric water content (VWC) and pressure heads at 10, 40, and 65 cm depth at P1. θ_{sat} is the saturated VWC (= 0.498). Black and white circles in 65 cm deep show the data that were applied and not applied to the calculation of VWC in the stability analysis shown in Figures 9 and 10, respectively. The correction curve is expressed as y = 0.11 + 0.24 e $^{0.23x}$ (r = 0.99) for the VWC below 0.31.

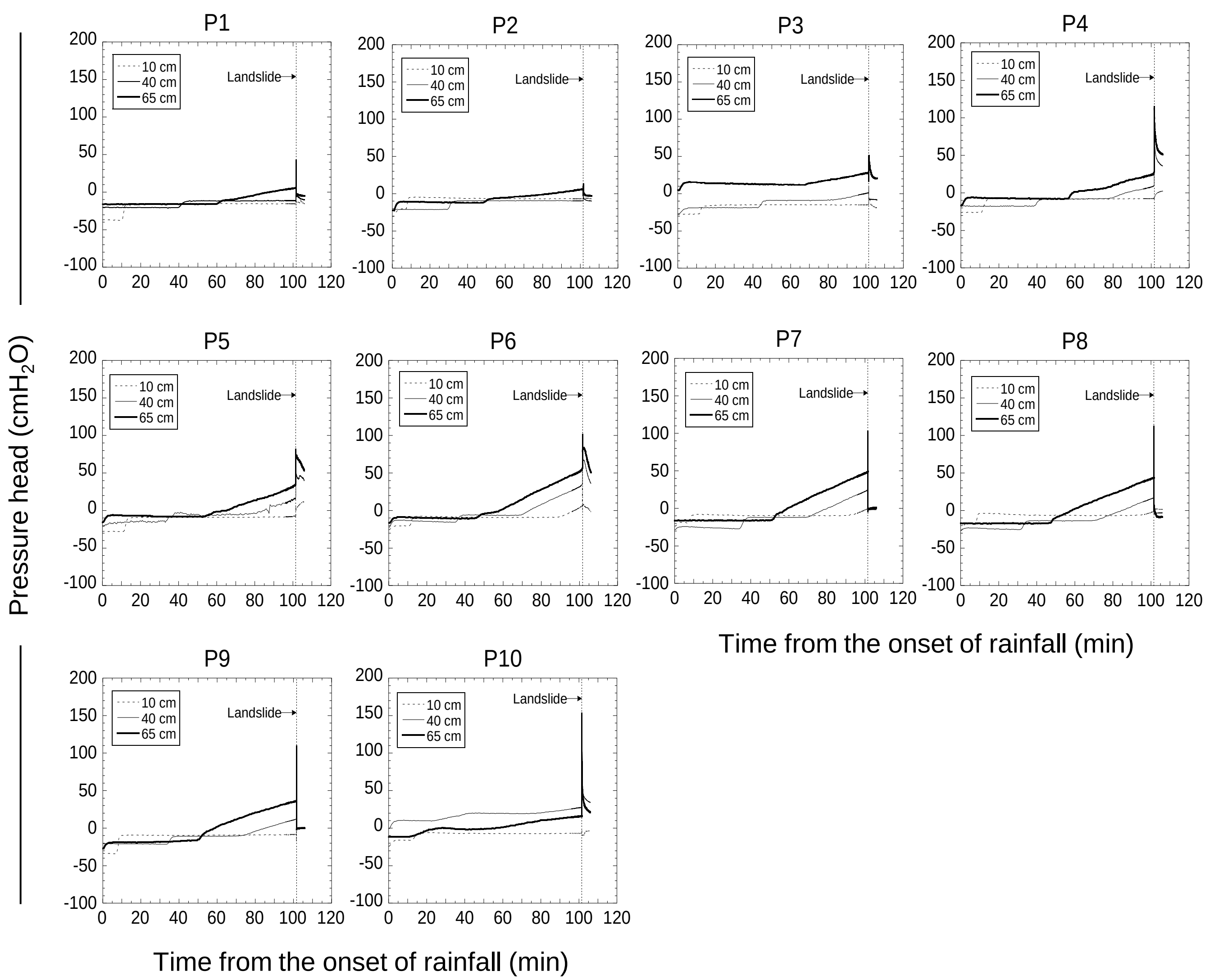

Figure 4. Changes in pore water pressures.

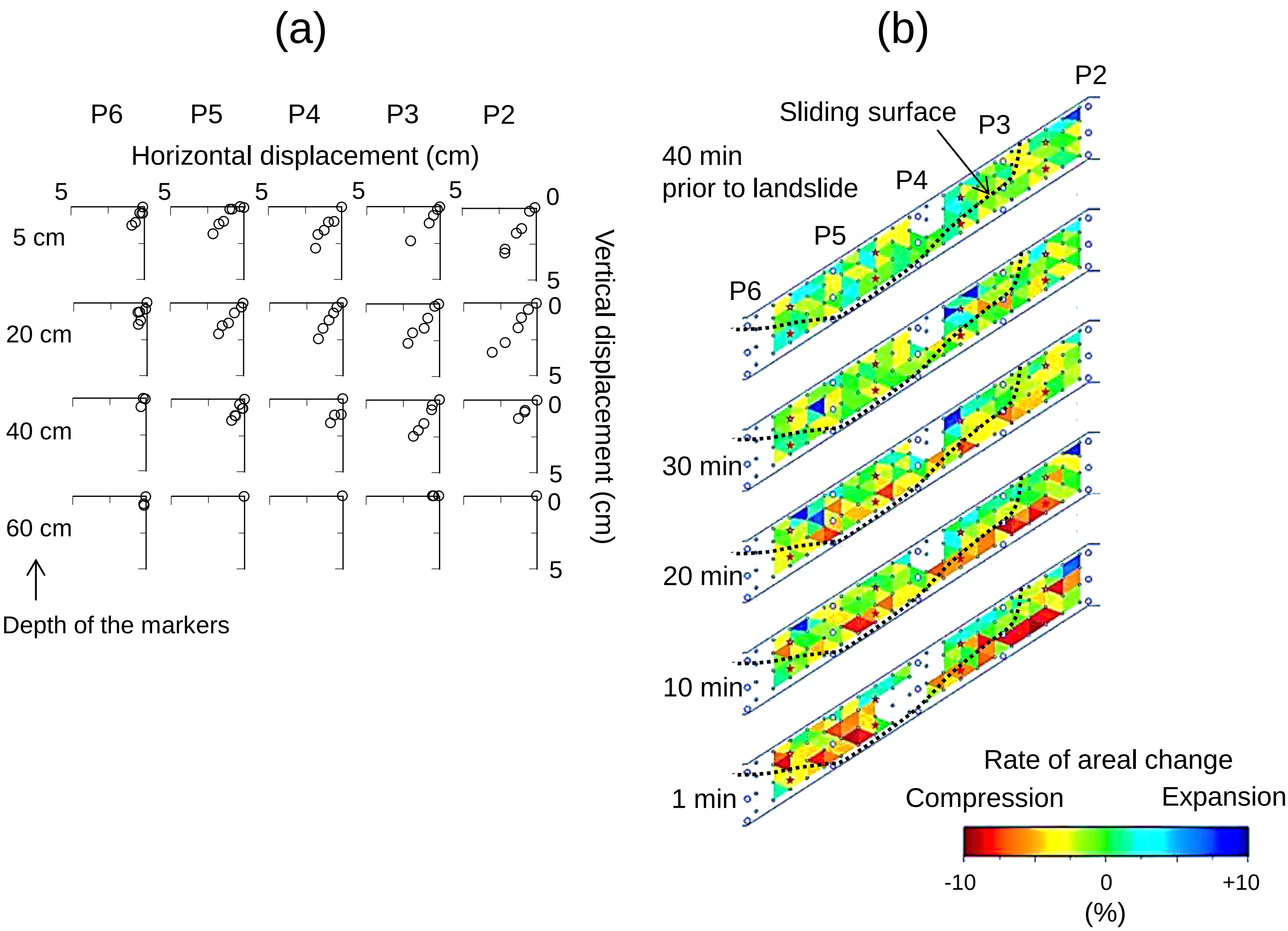

Figure 5. Soil displacement (loci of the markers) at P2 – P6 at 50, 40, 30, 20, 10, and 1 min prior to landslide (a) and the rate of areal change in triangles (b) in the upper steep slope, based on the position of the cylindrical markers. The origin in (a) shows the initial position of the markers before the onset of rainfall. The rate of areal change (b) was calculated from the comparison of the area of triangles at each time with that before the onset of rainfall. The areal change (or soil displacement) was not observed before 50 min prior to landslide. White color around P4 in (b) shows no data because of the noise of video imagery.

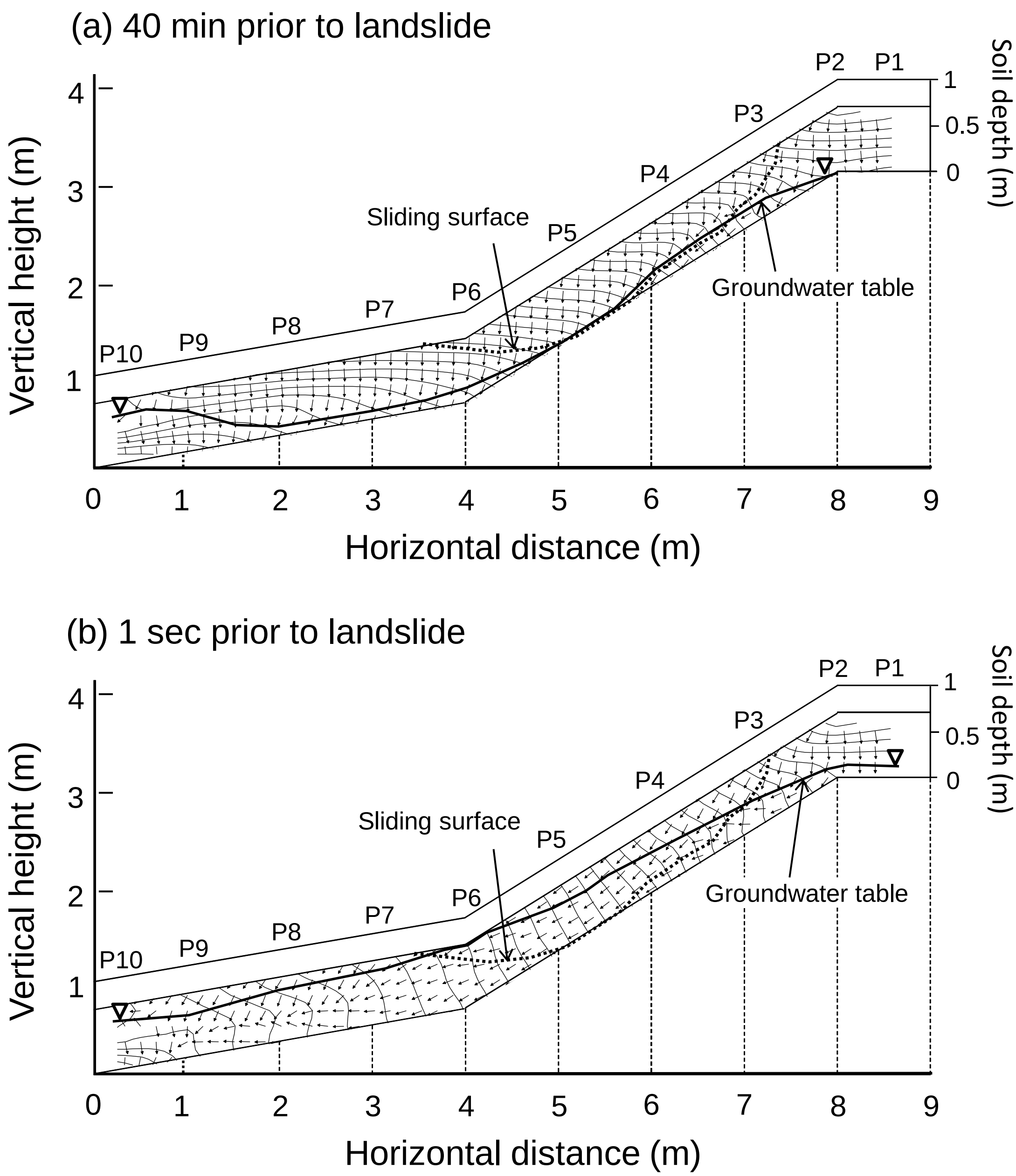

Figure 6. Temporal changes in the equi-potential lines and the directions of subsurface flow (arrows) prior to landslide. Contour intervals of the equi-potential lines are 20 cm H_2O.

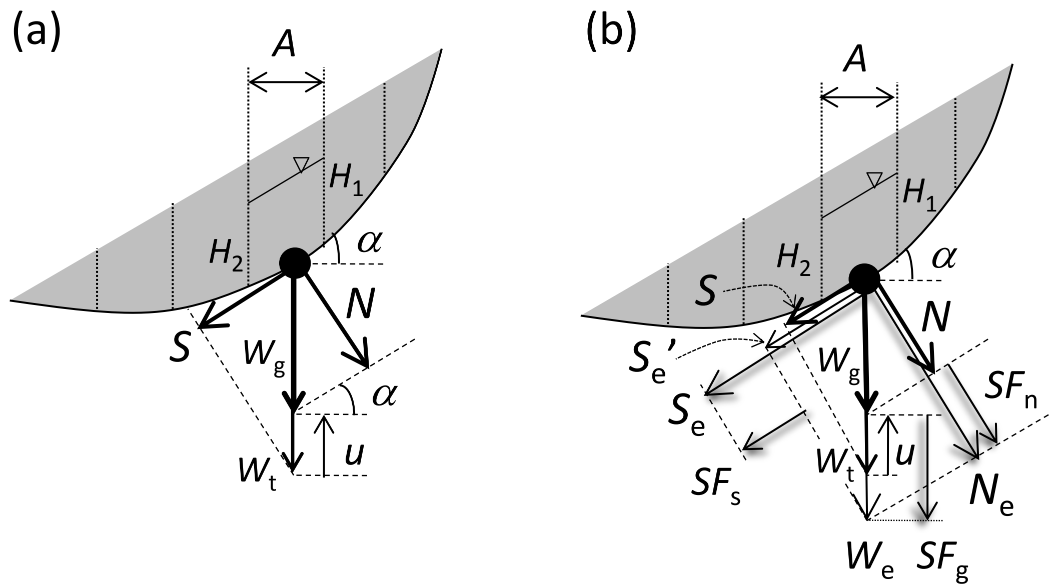

Figure 7. Schematic illustrations related to inner forces affecting a slice of landslide masses under a free ground water condition.

(A) Modified Fellenius method without considering seepage force;

where A is the plan area of the slice, H_1 and H_2 are the pore water pressures at the up and down sides of the slice, respectively, W_g (eq.3) is the effective weight of soil considered the buoyancy, W_t (eq.1) is the total weight of soil, u (eq.3) is the buoyancy, α is the average slope of sliding surface in the slice, N (eq.2) is normal force, and S (eq.1) is shear force parallel to the sliding surface in the slice.

(B) Our proposal applied seepage forces for vertical and slope parallel directions;

where W_e (eq.13) is the effective weight of soil considered the buoyancy and vertical seepage force, SF_g (eq.9) is seepage force to a vertical direction combined the effect of saturated and unsaturated subsurface flows, SF_n (eq.11) is seepage force fraction of SF_g in the normal direction, N_e (eq.12) is effective normal force, S_e' (eq.14) is effective shear force resulted from the appearance of SF_g, SF_s (eq.16) is seepage force parallel to the sliding surface, and S_e (eq.15) is effective shear force parallel to the sliding surface in the slice.

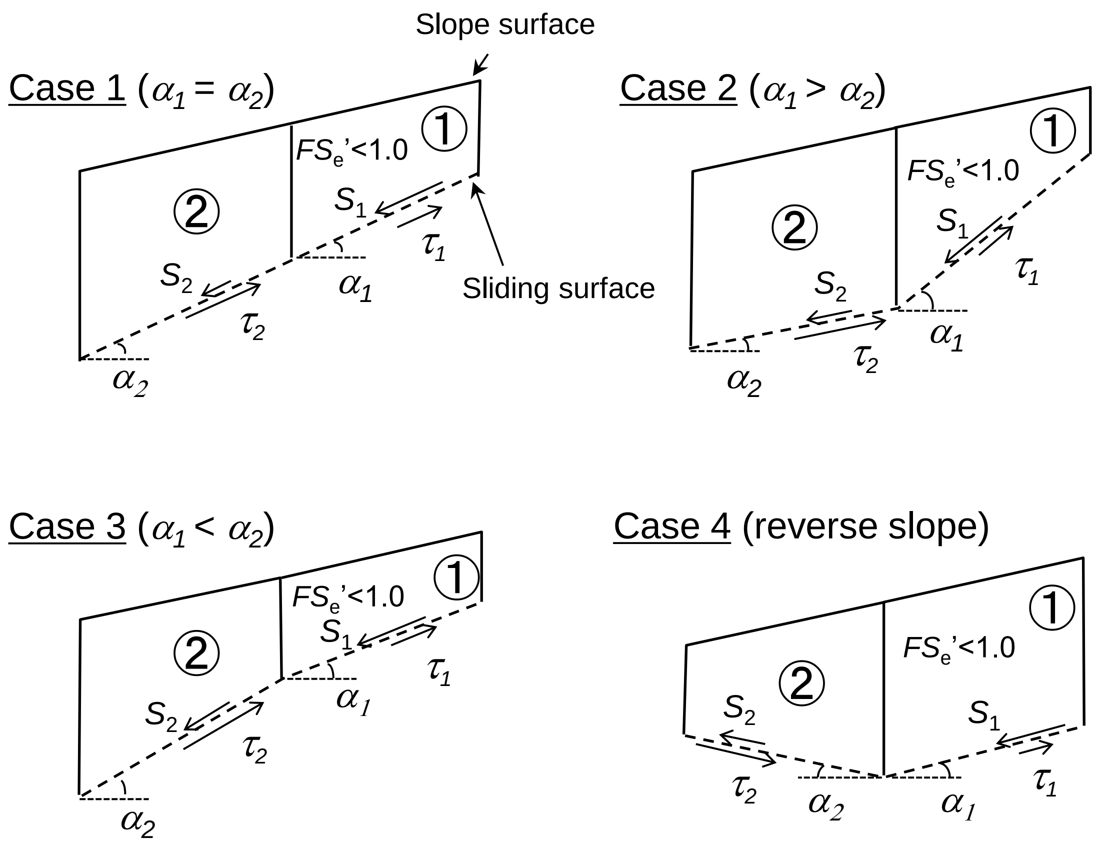

Figure 8. Types of the interrelationship regarding the slope of sliding surface between the slices. FS_e' (eq.17) is the factor of safety taking into account apparent soil cohesion and seepage force but not transferring the excess shear force from the adjacent up-slope landslide segment, α is the slope of sliding surface, and S and τ are shear force and shear resistance operating to the sliding surfaces of the slices, respectively.

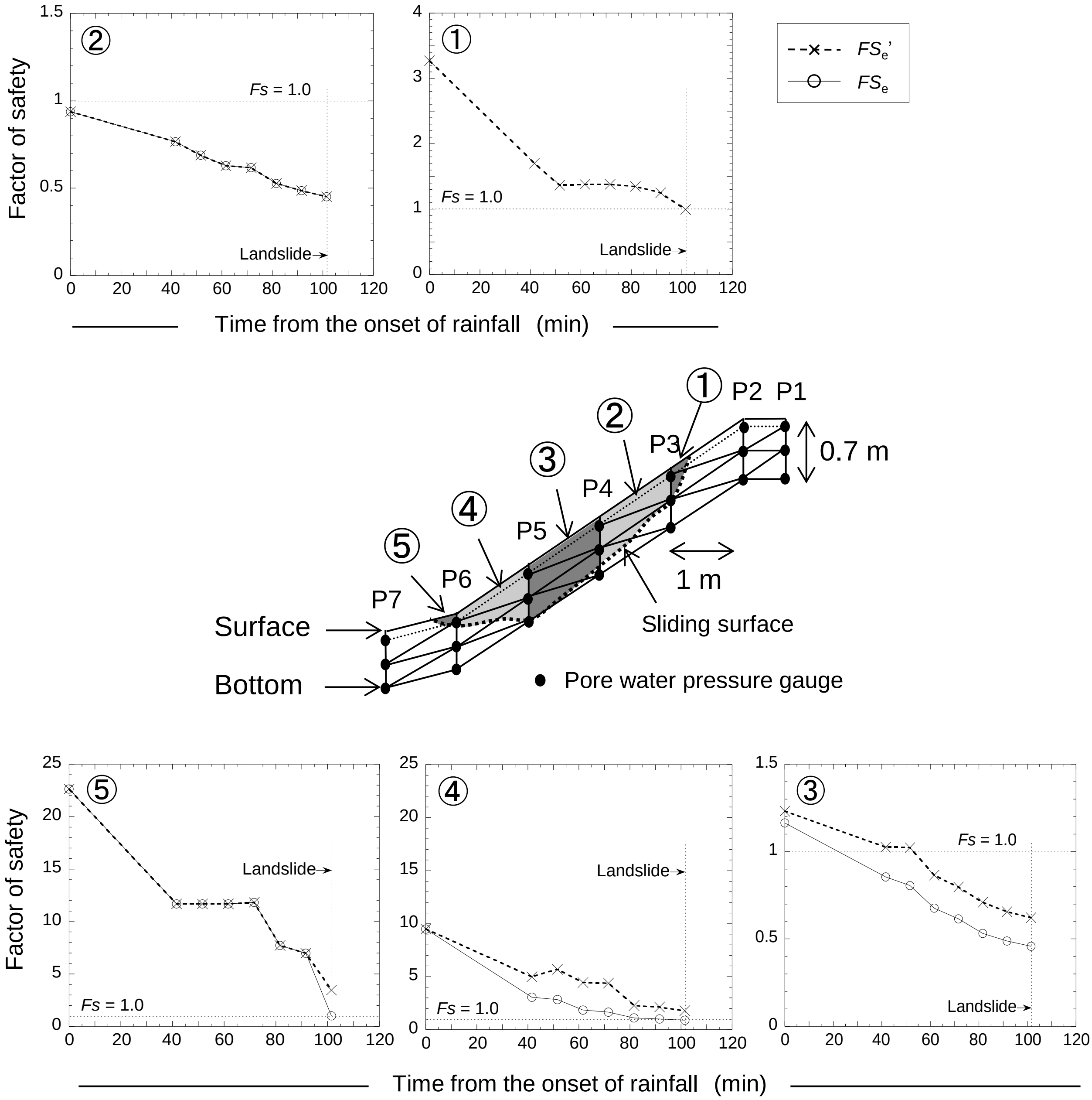

Figure 9. Changes in the factor of safety. FS_e' (eq.17) is the factor of safety not taking into account the excess shear force and FS_e (eq.20) is the factor of safety transferred the excess shear force from the up-slope segment.

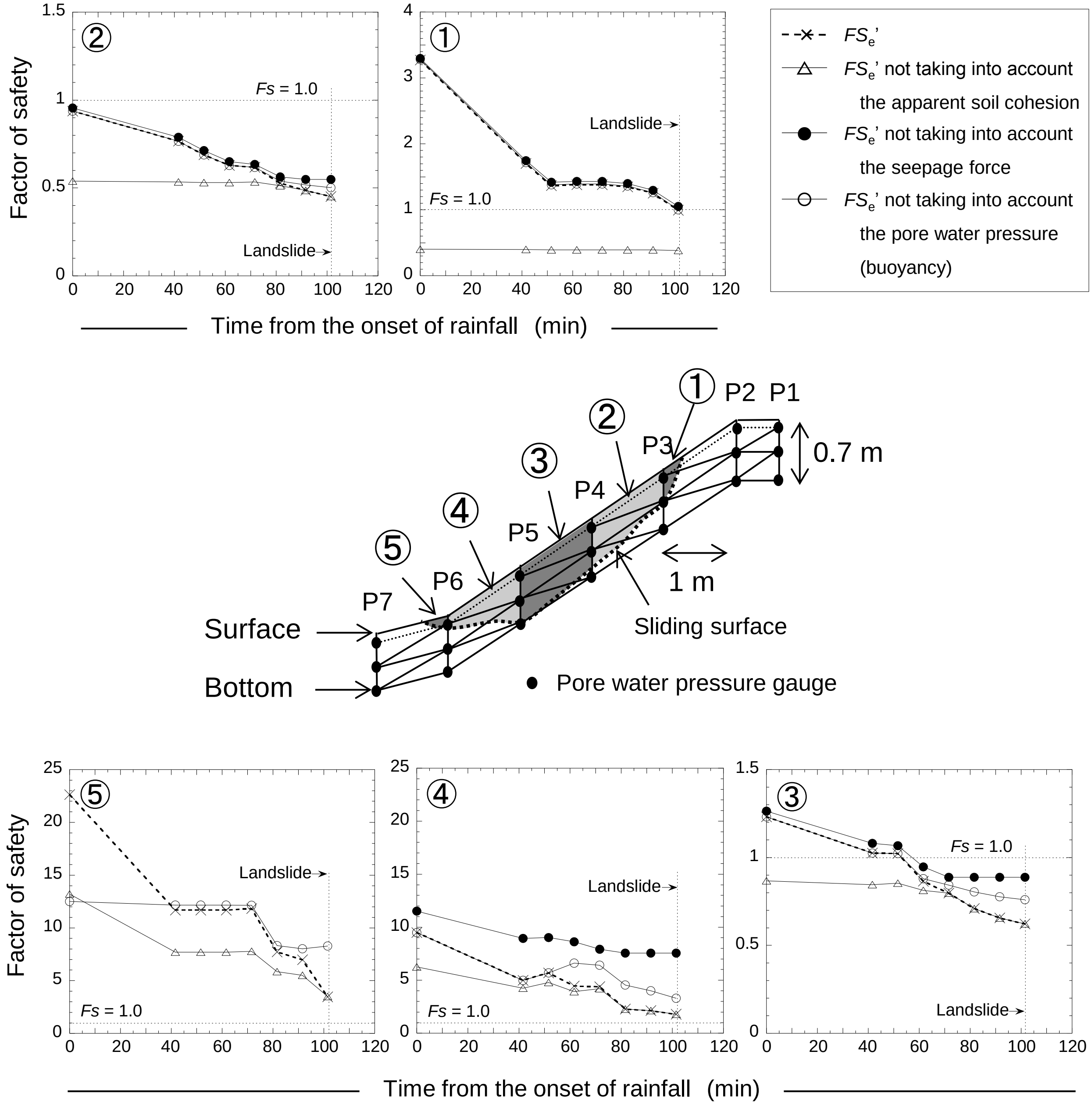

Figure 10. Effects of each force on shallow landslide initiation. FS_e' (eq.17) is the factor of safety not taking into account the excess shear force.

Table 1. Physical properties of the experimental sand (arithmetic mean of 5 samples)

Density : ρ_s (g cm^{-3})	2.57
Dry density : ρ_d (g cm^{-3})	1.29
Void ratio : e	0.99
Saturated soil water content : θ_{sat} (cm^3 cm^{-3})	0.498
Saturated hydraulic conductivity : K_{sat} (cm s^{-1})	3.1×10^{-2}
Median diameter : D_{50} (mm)	0.39
Angle of internal friction : ϕ_{cd} (°)	32.6
Soil cohesion : c_{sat} (gf cm^{-2})	0